JPE 19-4-16

https://doi.org/10.6113/JPE.2019.19.4.1011
ISSN(Print): 1598-2092 / ISSN(Online): 2093-4718

Buck-Flyback (fly-buck) Stand-Alone Photovoltaic System for Charge Balancing with Differential Power Processor Circuit

Chun-Gu Lee*, Jung-Hyun Park*, and Joung-Hu Park†,*

†,*Department of Electrical Engineering, Soongsil University, Seoul, Korea

Abstract

In this paper, a buck-flyback (fly-buck) stand-alone photovoltaic (PV) system for charge balancing with a differential power processor (DPP) circuit is proposed. Conventional feed-back DPP converters draw differential feed-back power from the output of a string converter. Therefore, the power is always through the switches and diodes of the string converter. Because of the returning conduction path, there are always power losses due to the resistance of the switch and the forward voltage of the diode. Meanwhile, the proposed feed-back DPP converter draws power from the magnetically-coupled inductor in a string converter. This shortens the power path of the DPP converter, which reduces the power losses. In addition, the extra winding in the magnetically-coupled inductor works as a charge balancer for battery-stacked stand-alone PV systems. The proposed system, which uses a single magnetically-coupled inductor, can control each of the PV modules independently to track the maximum power point. Thus, it can overcome the power loss due to the power path. It can also achieve charge balancing for each of the battery modules. The proposed topology is analyzed and verified using 120W hardware experiments.

Key words: Buck-flyback, Charge balancing, Differential power processor, Fly-buck converter, Forward converter, Photovoltaic applications

I. INTRODUCTION

Among renewable energy resources, solar energy has been put in the spot light. Systems using solar energy have some advantages since the generators are small in size, low in weight and easy to expand. Due to these advantages, solar energy applications such as photovoltaic systems can be used for a wide power range from small power residential applications up to large mega-watt power solar farms [1]-[3]. Because solar panels have low voltage high current output characteristics, they are connected in series the early stage. However, in the case of a simple serial structure, the overall system efficiency is low due to partial shading, and the entire system cannot operate even if one panel is in trouble [4]-[6].

To solve this problem, the module integrated converter (MIC) was proposed. In the MIC, while the whole manufacturing cost is more expensive than that of conventional centralized photovoltaic structures, it can control each PV panel independently which solves the problem of poor efficiency due to partial shading and the system operation problem due to partial failures [7]-[13].

The differential power processor (DPP) was recently proposed to overcome the disadvantages of the MIC while maintaining its advantages. Fig. 1 shows the DPP converter structure. It is different from the MIC since a converter is connected with each solar panel in parallel while the PV panels are connected in series. The DPP converter topology is divided into two types depending on the DPP power flow. One is the feed-forward DPP converter and the other is the feed-back DPP converter. Fig. 2 shows a feed-forward type DPP converter, and Fig. 3 shows a feed-back type DPP converter. In the feed-forward type, when the output power of a certain panel is higher than that of the other panels, the power difference between the high output panel and the other panels is transferred directly to the output of string converter through a DPP converter. As shown in Fig. 2, when the PV1 output power is 30W and the other PV panels are all 20W under the

Manuscript received Aug. 10, 2018; accepted Mar. 18, 2019
Recommended for publication by Associate Editor Seongjun Lee.
†Corresponding Author: wait4u@ssu.ac.kr
Tel: +82-2-820-0645, Fax: +82-827-7961, Soongsil University, Korea
*Dept. of Electronic Eng., Soongsil University, Korea

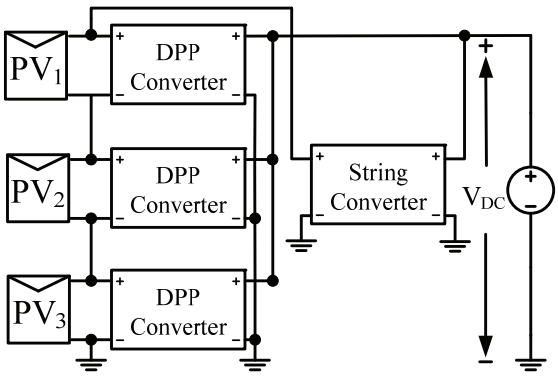

Fig. 1. Differential power processing (DPP) converter structure.

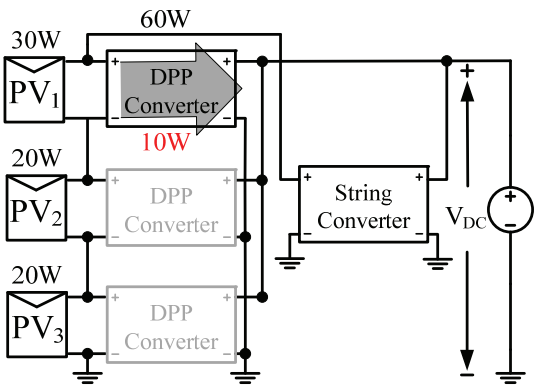

Fig. 2. Feed-forward DPP converter structure.

same voltage, 10W of the PV1 power is transferred to the output of a string converter through a DPP converter. In the feed-back type, when the output power of a certain panel is lower than the other panels, the power difference between the low power panel and the other panels is transferred back to the low power panel to compensate its low power through a DPP converter. As shown in Fig. 3, when the PV1 output power is 10W and the other PV panels are all 20W, 10W of the string converter power is transferred to the output of PV1 through a DPP converter with the same MPP voltage. The feed-forward and feed-back DPP converters are totally different from the MICs because they operate only when there is a power difference between PV panels. Thus, there are no power losses under full radiations, which overcomes the loss and cost problems of the MIC. In addition, it relieves an aging problem.

However, there is a significant difference between the feed-forward DPP converter and the feed-back converter. From the perspective of system efficiency optimization, it seems advantageous to use a feed-forward DPP converter. The feed-forward DPP converter delivers differential power directly to the output through the DPP converter, while the feed-back DPP converter delivers the necessary power back to the PV input from the string converter through the DPP converter. This means that the power flow path of the feed- forward is

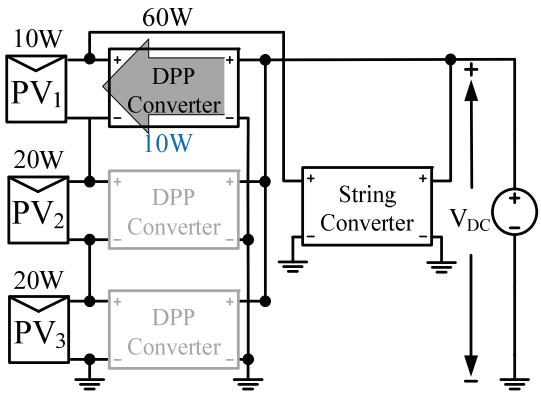

Fig. 3. Feed-back DPP converter structure.

shorter than that of the feed-back DPP converter. However, since PV systems are usually installed in environments where very few PV panels are shaded, and shading occurs rarely to produce power maximally, all of the feed-forward DPP converters, except for a DPP with shaded panels, transfer the extra power. Meanwhile, feed-back DPP converters in this situation have just one or two in operation. Considering the environment, it is reasonable to use feed-back type DPP converters to optimize system efficiency.

A buck-flyback (fly-buck) stand-alone PV system for charge-balancing with DPP circuit is proposed in this paper. This stand-alone system uses the feed-back DPP converter structure to track the maximum power point of a PV panel. However, the proposed feed-back DPP converter uses a magnetically-coupled inductor to overcome the long power path problem of the conventional feed-back DPP converter structure. In the proposed feed-back DPP, the DPP power for maximum power generation is not transferred through the output of the string converter (battery side). Instead it is transferred through the magnetically-coupled inductor in the middle of the string converter. Furthermore, a typical stand-alone PV-battery charger uses additional DC-DC converters controlled for charge balancing. Meanwhile, the proposed system uses a coupled inductor for the balancing instead of an additional DC-DC converter. The proposed string converter has some extra windings in the magnetically-coupled inductor for charge balancing. This works as a secondary equally-multi-winding flyback for equalizing the secondary battery module voltages. Since an additional DC-DC converter is not used, the topology is very cost-effective and easy to use without a controller [14], [15].

The proposed topology is verified by 120W prototype hardware experiments. The paper is organized as follows. Section II explains the structure of the proposed topology along with a functional classification and explanation. Section III presents design guidelines along with formulas. Section IV shows the experimental specification and experimental results. Finally, section V presents some conclusions.

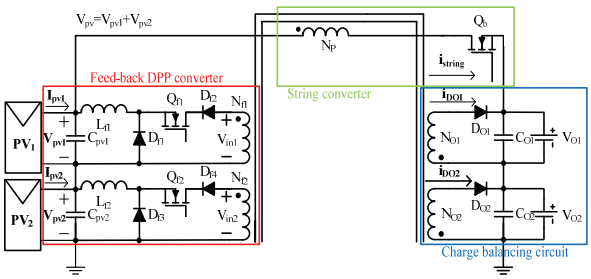

Fig. 4. Equivalent circuit model of the proposed converter in a single-core 5-winding coupled-inductor.

II. Operating Principle

A. Structure of the Proposed Converter

Fig. 4 shows a circuit diagram of the proposed power conditioning system topology. The proposed power conditioning system consists of a string converter, DPP converters and charge-balancing circuitry. The proposed converter operates through the main switch Q_b and the switches Q_{f1} and Q_{f2} of the DPP converter.

V_{O1} and V_{O2} are the output battery voltage, which is almost fixed. Thus, the total PV voltage V_{PV} is regulated by the main switch Q_b in the string converter.

When a power deviation occurs between PV_1 and PV_2, one of the switches Q_{f1} or Q_{f2} is in the rest state, and the other is switched to regulate the corresponding PV voltage through the inductor voltage V_L, which is determined by N_{f1} or N_{f2}. In the operation of the above DPP converter, the critical principle is that the DPP converter input voltage is induced through the coupled inductor while the string switch Q_b turns on. Thus, Q_b should stay turned on until Q_{f1} and Q_{f2} are turned off. Therefore, the duty ratio of Q_b in the buck-flyback (fly-buck) converter must be greater than that of the DPP (Q_{f1} or Q_{f2}) under synchronization [16].

The anode voltages of the diodes D_{O1} and D_{O2} are half of the output voltage determined by N_{O1} or N_{O2}. When there is an imbalance between the battery voltages, D_{O1} or D_{O2} turns on because of the cathode voltage difference between the diodes sharing the anode voltages through the winding N_{O1} and N_{O2}. The secondary balancing circuit shares a switch with the string converter. The string converter charges the batteries when the switch Q_b is on. In addition, the balancing circuit charges the minimally charged battery unit when Q_b is off.

B. Operating Principles

There are three operating modes when the proposed converter is operated under the continuous conduction mode (CCM). Assume the PV modules are series connected, where the maximum power of PV_1 is greater than that of PV_2. The solid black line in Figure 5 means the conduction path.

Mode 1: In Fig. 5(a), the DPP converter with PV_2 is operated while the other DPP is off because of the difference between the MPP current of PV_1 and that of PV_2. The sum of

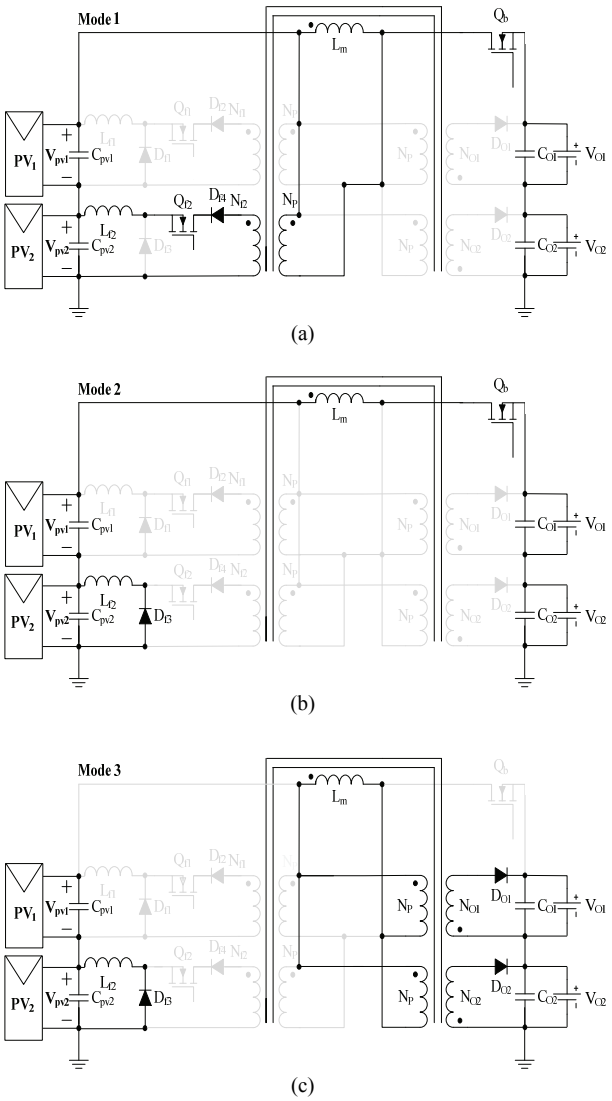

Fig. 5. Operating modes of the proposed converter. (a) Q_b on, Q_{f2} on [0~D_PT]. (b) Q_b on, Q_{f2} off [D_PT~D_bT]. (c) Qb on, Qf2 off [D_bT~Ts].

the voltages of PV_1 and PV_2 is applied to the primary of the coupled inductor when Q_b is turned on. Then the inductor primary voltage is applied to the DPP converter input with the turn ratio $\frac{N_{f2}}{N_p}$. Then the switch Q_{f2} is turned on, which supplies current to PV_2 in order to compensate the small MPP current to match the string current. All of the power from the PVs instantaneously charged the battery units.

Mode 2: In Fig. 5(b), Q_{f2} is turned off and Q_b stays on. The diode D_{f2} is turned on and the L_{f2} current freewheels through the diode.

Mode 3: In Fig. 5(c), Q_b is turned off and the diode (D_{O1} or D_{O2}) with the lower voltage battery is turned on. Magnetizing inductor current flows through the diode and charges the battery unit. The off-time flyback operation only compensates the lower-charged battery to equalize the battery voltages.

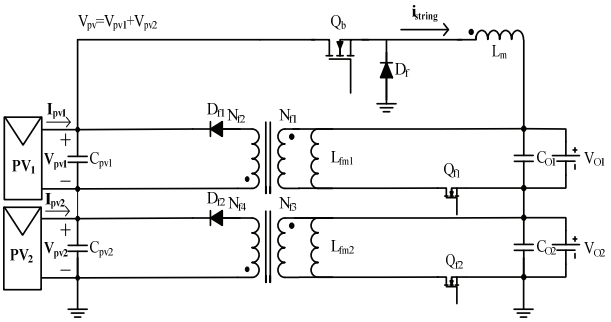

Fig. 6. Conventional flyback DPP converters with a buck-type string converter.

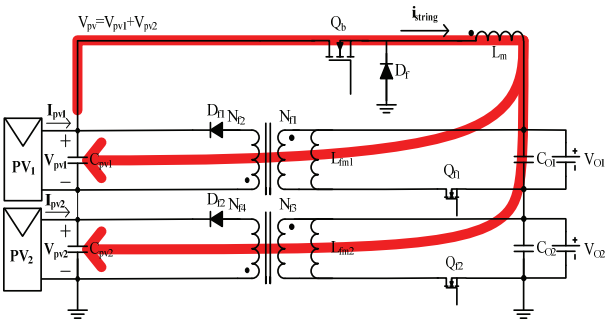

Fig. 7. DPP power flow of the conventional converter topology.

C. DPP Converter Feedback Power Path

Fig. 6 shows a conventional feedback-type DPP flyback converter circuit. The input of the conventional DPP circuit is the battery stack for stand-alone PV operation, and the output of the conventional DPP flyback is the PV module. The DPP converters can operate independently. Therefore, when a PV partial-shading or a failure occurs, the DPPs allow each of the modules to continue to operate at the maximum power points (MPPs). However, since the input of the conventional DPP topology is the output of the string converter, the DPP must be designed for a high step-up gain. This gain results in large losses and a high cost. The high step-up converter requires a high on-resistance transistor for Q_f, which results in a decrease in efficiency. Fig. 7 has an arrow showing the power flow in the system. The conventional DPP circuit transfers power through the output of the string converter, which results in some power losses due to the parasitic resistance of Q_b, L_m, G_{fl}, N_{p1} and so on. In order to overcome the loss problem, a new DPP topology is proposed. Like the previously mentioned DPP in the feedback mode, the proposed DPP transfers power to the PV module only when the PV current is less than that of the string. Fig. 8 has an arrow to show the power flow in the proposed DPP converter. In this topology, the DPP circuit input is not the output of the string converter. It is the tertiary windings of the magnetically-coupled string inductor. Since the power for the DPP bypasses the string converter, there are fewer power losses due to the parasitic resistances of the string. In addtion, the on-resistances of the DPP switches (Q_{fl} and Q_{f2}) are small due to the low voltage

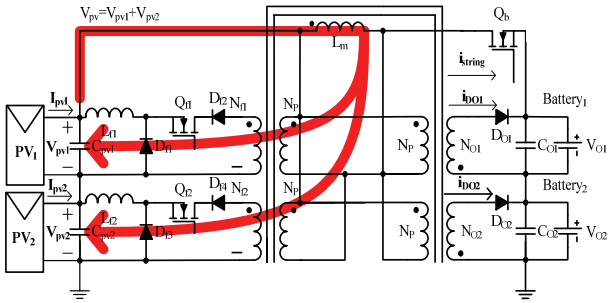

Fig. 8. DPP Power flow of the proposed converter.

stress, which contributes to the high efficiency. Furthermore, by the extended version of the coupled inductor, the tertiary winding (N_{O1} and N_{O2}) can do the charge-balance among the battery units without extra charge-balancing circuits since the balancing circuit operation is totally decoupled.

D. Charge Balance for a Battery Stack

If there is an imbalance between battery voltages, one of the tertiary diodes starts to conduct. When the switch Q_b is turned off, the diodes D_{O1} and D_{O2} are turned on and off repeatedly according to the battery voltages for charge balancing [17]. When the switch Q_b is turned off, the diode current I_{DO1} is derived as equation (1), under an assumption that the voltage of battery-2 (V_{O2}) is higher than that of battery-1 (V_{O1}).

$$I_{D_{O1}} = \frac{\int_{DT}^{D_P T} (i_{L_m} \cdot \frac{N_P}{N_{O1}}) dt}{T} \tag{1}$$

where D_P is the main duty-ratio plus the conduction ratio of the diode current I_{Do1} during the off time, and i_{Lm} is the magnetizing current. N_P is the turn ratio of the primary side of the magnetically-coupled inductor, and N_{O1} is the tertiary winding.

I_{DO1} depends on the load imbalance as follows:

$$I_{D_{O1}} = I_{batt2} - I_{batt1} \tag{2}$$

Equation (3) is derived from equations (1) and (2) as follows:

$$\begin{aligned} I_{batt2} - I_{batt1} &= \frac{\int_{D_b T}^{D_P T} \left(i_{L_m} \cdot \frac{N_P}{N_{O1}} \right) dt}{T} \\ &= (D_P - D_b) \cdot \left(I_{L_m} \cdot \frac{N_P}{N_{O1}} \right) \end{aligned} \tag{3}$$

where I_{Lm} is the average current of the magnetically-coupled inductor.

In equation (3), I_{Lm} can be replaced by I_{PV1} / D_b, where I_{PV1} is the average current of PV_1. Therefore, equation (4) is derived from equation (3) as follows:

$$\begin{aligned} I_{batt2} - I_{batt1} &= (D_P - D_b) \cdot \left(\frac{I_{PV_1}}{D_b} \cdot \frac{N_P}{N_{O1}} \right) \\ &= \left(\frac{D_P}{D_b} - 1 \right) \cdot I_{PV_1} \cdot \frac{N_P}{N_{O1}} \end{aligned} \tag{4}$$

Then D_P is derived as equation (5) from equation (4). Since

the duty cycle should exist between $0 \le D_P \le 1- D_b$, equation (6) is derived from equation (5).

$$D_P = D_b \cdot ((I_{batt2} - I_{batt1}) \cdot \frac{1}{I_{PV_1}} \cdot \frac{N_{O1}}{N_P} + 1) \quad (5)$$

$$0 \le D_b \cdot ((I_{batt2} - I_{batt1}) \cdot \frac{1}{I_{PV_1}} \cdot \frac{N_{O1}}{N_P} + 1) \le 1 - D_b \quad (6)$$

From equation (6), the limit of the imbalance load current (I_{DO1} = I_{batt2} - I_{batt1}) that this balancer can compensate maximally is derived by equation (7).

$$-I_{PV_1} \cdot \frac{N_P}{N_{O1}} \le \cdot ((I_{batt2} - I_{batt1}) \le (\frac{1}{D_b} - 2) \cdot I_{PV_1} \cdot \frac{N_P}{N_{O1}} \quad (7)$$

In equation (7), the left term is negative, which is meaningless. Finally, equation (8) is derived as shown below.

$$0 \le I_{batt1} - I_{batt2} \le (\frac{1}{D_b} - 2) \cdot I_{PV_1} \cdot \frac{N_P}{N_{O1}} \quad (8)$$

From equation (8), the performance limit of the battery-voltage balancer is derived. Then it is used for the design constraint of the balancing circuit.

III. Design Guidelines

A. Design of the Fly-Buck Converter

In the CCM, the input voltage of the buck-flyback (fly-buck) string converter is determined by the duty ratio D_b of Q_b and the battery stack voltage [15]. The duty ratio D_b of an arbitrary n-module system is derived as equation (9) by the voltage-second balance of the magnetizing inductor. In addition, the n^{th} PV module output voltage is the input voltage of the n^{th} DPP converter. Under the CCM, the n^{th} DPP converter duty ratio $D_{f(n)}$ is derived by equation (10).

$$D_b = \frac{N_P}{\frac{\sum V_{PV(n)}}{\sum V_{O(n)}} \cdot nN_O + N_P - nN_O} \quad (9)$$

where $V_{PV(n)}$ is the voltage of each panel, $V_{O(n)}$ is voltage of each battery, N_O is tertiary winding, and n is the number of outputs.

$$D_{f(n)} = \frac{V_{PV(n)}}{\sum V_{PV(n)} - \sum V_{O(n)}} \cdot \frac{N_P}{N_{f(n)}} \quad (10)$$

Another constraint, the duty cycle D_b must be greater than $D_{f(n)}$. Therefore, design equation (11) is derived from equations (10) and (9).

$$\frac{N_P}{\frac{\sum V_{PV(n)}}{\sum V_{O(n)}} \cdot nN_O + N_P - nN_O} > \frac{V_{PV(n)}}{\sum V_{PV(n)} - \sum V_{O(n)}} \cdot \frac{N_P}{N_{f(n)}} \quad (11)$$

B. Inductor Design of the Proposed Converter

In the string converter, Δi_{Lm} is defined as equation (12), where $N_{O(n)}/N_P$=n, n is the number of outputs. In addition, the output voltage is balanced.

$$\Delta i_{L_m} = \frac{\left(\sum V_{PV(n)} - \sum V_{O(n)} - \frac{\sum V_{O(n)}}{n}\right) D_b T}{L_m} = \frac{nV_O\left(1 - D_b - \frac{D_b}{n^2}\right)}{L_m f} \quad (12)$$

The condition for the string converter to operate in the CCM is equation (13).

$$I_{L_m} - \frac{\Delta i_{L_m}}{2} \ge 0 \quad (13)$$

Equation (14) is derived from equations (12) and (13).

$$I_{L_m} - \frac{nV_O\left(1 - D_b - \frac{D_b}{n^2}\right)}{L_m f} \ge 0 \quad (14)$$

Equation (15), derived from equation (14), can be used to design the magnetizing inductance of the string converter (fly-buck), which is derived from the CCM condition, where PO is the output power of the converter, and *f* is the switching frequency of Q_b.

$$L_m \ge \frac{nV_O\left(1 - D_b - \frac{D_b}{n^2}\right)}{I_{L_m} f} \quad (15)$$

In the DPP converter, $\Delta i_{Lf(n)}$ is defined as equation (16).

$$\Delta i_{L_{f(n)}} = \frac{\left(\frac{N_{f(n)}}{N_P} \cdot (\sum V_{PV(n)} - \sum V_{O(n)}) - V_{PV(n)}\right) D_{f(n)} T}{L_{f(n)}} = \frac{(1 - D_{f(n)}) V_{PV(n)}}{L_{f(n)} f} \quad (16)$$

The condition for the DPP converter to operate in the CCM is equation (17).

$$I_{L_{f(n)}} - \frac{\Delta i_{L_{f(n)}}}{2} \ge 0 \quad (17)$$

Equation (18) is derived from equations (16) and (17).

$$I_{L_{f(n)}} - \frac{(1 - D_{f(n)}) V_{PV(n)}}{2 L_{f(n)} f} \ge 0 \quad (18)$$

In the proposed converter, $I_{Lf(n)}$ is the current difference between I_{string} and $I_{PV(n)}$. Therefore, equation (19) is derived for the filter inductance design of the n^{th} DPP buck converter, where $I_{Lf(n)}$ is the inductor average current of the DPP, $I_{PV(n)}$ is the average current of the $PV_{(n)}$, f is the switching frequency, and I_{string} is the average current of the string converter.

$$L_{f(n)} \ge \frac{\left(1 - D_{f_{(n)}}\right) V_{PV(n)}}{2(I_{string} - I_{PV_{(n)}}) f} \quad (19)$$

IV. Experimental Results

A 120W hardware prototype is designed and built in the laboratory. Fig. 9 shows a picture of the prototype and Fig. 10 shows a photograph of the experiment setup. In addtion,

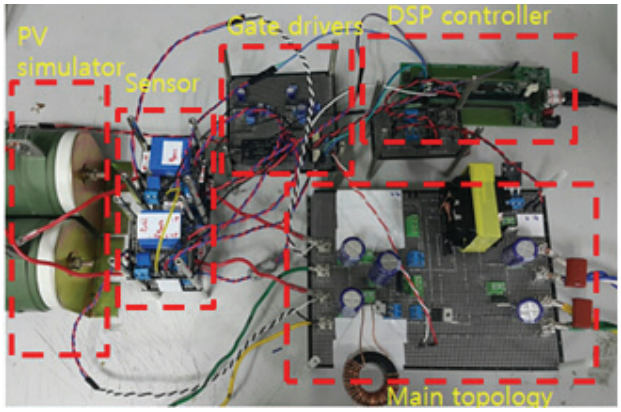

Fig. 9. Hardware prototype.

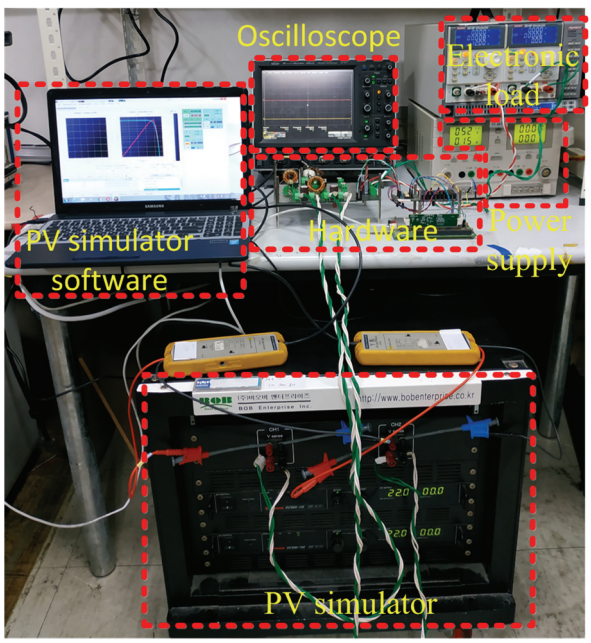

Fig. 10. Experimental setup.

Table I presents the design parameters of the hardware and Table II presents the hardware component part numbers. Fig. 11 shows the charge balancer output voltages, where V_{O1} is the yellow line and V_{O2} is the red line. In this figure, when there is an imbalance between V_{O1} and V_{O2}, the tertiary diodes connected to V_{O2} start to conduct to charge the battery. Therefore, V_{O1} and V_{O2} equally maintain an average voltage of around 12 V. Fig. 12 shows voltage and current waveforms of the hardware experiment. In Fig. 12(a), it is shown that the PV voltage and current waveforms change from a steady-state to another when an MPP step occurs. In this figure, on the left, the steady state of PV_1 is 20V, 3A and that of PV_2 is 19.5V, 2.8A. In this situation, the DPP converters do not operate since there is no need to compensate the PV current among the panels. After the step, on the right, PV_1 is 20V, 3.3A and PV_2 is 20V, 2.7A. Thus, the DPP converter start to operate to compensate the current difference, which makes the PV currents maintain the difference even though the

TABLE I
HARDWARE PARAMETERS

Parameters	Value	Parameters	Value
MPP of V_{PV1}, V_{PV2}	20 [VDC]	L_{f1}, L_{f2}	450 [uH]
I_{PV1}	3.3 A	I_{PV2}	2.7 A
V_{batt1}, V_{batt2}	12 [VDC]	C_{PV1}, C_{PV2}	200 [uF]
P_O	120 [W]	C_{batt1}, C_{batt2}	200 [uF]
F	50 [kHz]	$N_P : N_{f1} : N_{f2}$	1 : 4 : 4
L_m	150 [uH]	$N_P : N_{O1} : N_{O2}$	1 : 1 : 1

TABLE II
HARDWARE COMPONENT LIST

Components	Part
Q_b	IRFP4568
Q_{f1}, Q_{f2}	IRFP4568
Gate driver	TLP250
D_{f1}, D_{f2}, D_{f3}, D_{f4}	B40250
D_{O1}, D_{O2}	B40250
PV simulator	Elgar TerraSAS

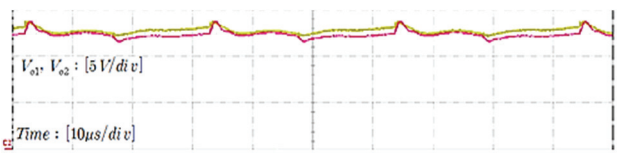

Fig. 11. Charge balancer output voltages.

voltages are kept similar. In addition, Fig. 12(b) shows drain-source voltage waveforms of Q_b ($V_{ds,\ string}$) and Q_f ($V_{ds,\ dpp}$). In Fig. 12(b), it can be seen that Q_{f2} turns on after Q_b turns on. It can also be seen that Q_{f2} turns off before Q_b turns off. Therefore, both of the switching operation are well matched when the synchronization of the coupled inductor was realized by a multi-inner winding coaxial-cabled single-core transformer, which contributes to the small spikes on the drain-source voltages through the small leakage inductance, as shown in Fig. 12(b). Fig. 12(c) shows an input voltage waveform of the DPP converter. In addition, Fig. 12(d) shows a current waveform of the inductor of the DPP converter and a voltage waveform of the inductor of the DPP converter.

Fig. 13 shows the MPP tracking (MPPT) operation of the proposed converter. The PV_1 and PV_2 MPPs are 20V. In Fig. 13, each PV voltage is sustained around 20V due to the DPP converter regulation and the P&O (perturb-and-observe) algorithm.

Equation (20) can be used to estimate the total system efficiencies of the proposed and conventional converters.

$$\eta_{total} = \frac{\left(P_{PV_1} + P_{PV_2}\right) + \left(P_{PV_1} - P_{PV_2}\right) \cdot \eta_{DPP} - \left(\frac{P_{PV_1} - P_{PV_2}}{\eta_{string}}\right)}{P_{PV_1} + P_{PV_2}} \quad (20)$$

where P_{PV1} and P_{PV2} are the PV output powers, and η_{DPP} and η_{string} are the efficiencies of each converter. Fig. 14 shows theoretically estimated and hardware measured efficiency

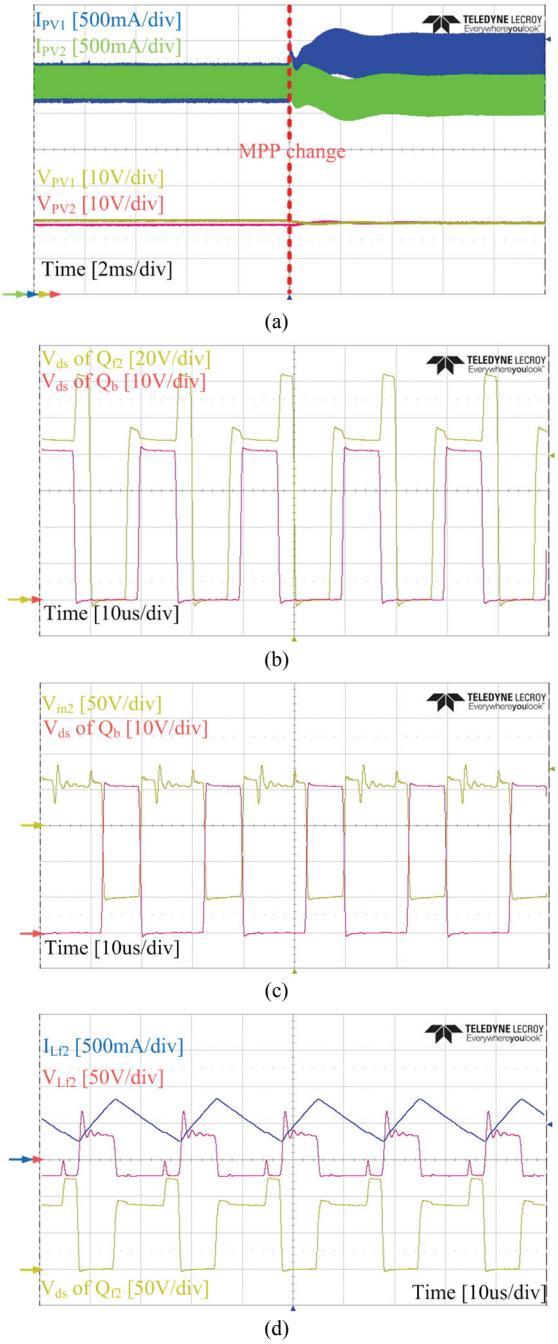

Fig. 12. Key waveforms of the hardware prototype. (a) $PV_{1,2}$ voltage and $PV_{1,2}$ current at an MPP step. (b) Switch drain-source voltage. (c) DPP input voltage; (d) DPP inductor voltage and DPP inductor current.

graphs of both the proposed converter and the conventional converter. In Fig. 14, it can be seen that the estimated and experimental efficiencies agree well each other. This means that equation (20) is available for the efficiency estimation. In addition, it can be seen that when the DPP power increases, both the conventional converter and the proposed converter efficiencies decrease since the DPP power circulates from the output to the input of the power conditioning systems, which results in some conduction losses. However, the efficiency

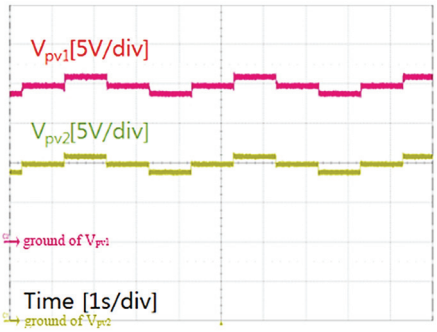

Fig. 13. Waveforms of the DPP converter output voltages (PV voltages) under MPP tracking operation.

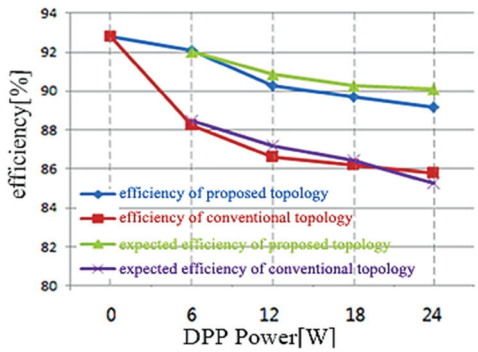

Fig. 14. Entire-system efficiency comparison between the proposed and conventional topologies according to the DPP power (power difference among the panels) variation.

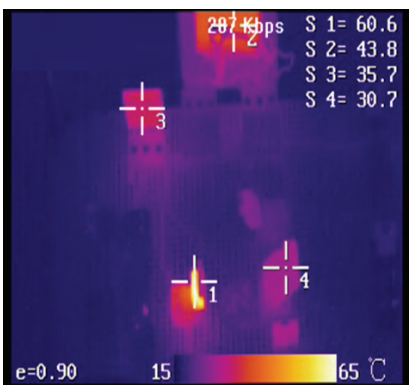

Fig. 15. Thermal camera image at a DPP power of 15W.

reduction of the conventional converter is greater than that of the proposed converter. This means that the proposed magnetically-coupled inductor reduces the power-loss increase when the power is transferred through the DPP converter since the circulating route is far shorter than that of the conventional case. Fig. 15 shows the temperature distribution of the main power devices when the proposed converter operates in the thermal steady-state. S1 shows the location of D_{O2}, S2 is the magnetically-coupled inductor, S3 is Q_b, and S4 is Q_{f2}. Fig. 15 shows that all the main power devices operate in the normal temperature range without any heat sinks which makes it feasible for real applications.

V. CONCLUSIONS

In this paper, a buck-flyback (fly-buck) DPP circuit stand-alone PV system with battery charge balancing is proposed. Because of the use of a single-core magnetically-coupled multi-winding inductor, the converter avoids a high step-up DPP converter design and the long-circulating path of conventional DPP topologies. Hence, the proposed converter is more power-efficient and cost-effective when compared to conventional converters. In addition, the proposed converter has a simple charge-balancing circuit composed of tertiary windings for the battery stacks in stand-alone systems. This balancing circuit operates in a passive manner like flyback multi-winding balancers. As a result, no additional control is necessary. In addtion, due to the DPP converters, this topology can operate independent MPPT control even under partial shading conditions. The proposed topology was analyzed and a design guideline was presented. In addition, they were validated using a 120W hardware prototype.

ACKNOWLEDGMENT

This research was supported by Korea Electric Power Corporation (Grant number: R17XA05-54).

REFERENCES

[1] P. Fairley, "Big solar's big surge," *IEEE Spectrum*, Vol. 52, No. 1, pp. 41-44, Jan. 2015.

[2] M. S. Irfan, J.-H. Shin, and J.-H. Park, "New control method for power decoupling of electrolytic capacitor-less photovoltaic micro-inverter with primary side regulation," *J. Electr. Eng. Technol.*, Vol. 13, No. 2, pp. 677-687, Mar. 2018.

[3] C. Kim, "An improved photovoltaic system output prediction model under limited weather information," *J. Electr. Eng. Technol.*, Vol. 13, No. 5, pp. 1874-1885, Sep. 2018.

[4] M. S. Manoharan, A. Ahmed, J.-W. Seo, and J.-H. Park, "Power conditioning for a small-scale PV system with charge-balancing integrated micro-inverter," *J. Power Electron*., Vol. 15, No. 5, pp. 1318-1328, Sep. 2015.

[5] S.-J. Park, J.-H. Shin, J.-H. Park, and H.-J. Jeon, "Dynamic analysis and controller design for standalone operation of photovoltaic power conditioners with energy storage," *J. Elect. Eng. Technol*., Vol. 9, No. 6, pp. 2004-2012, Nov. 2014.

[6] M. S. Manoharan, A. Ahmed, and J.-H. Park, "Peak-valley current mode controlled H-bridge inverter with digital slope compensation for cycle-by-cycle current regulation," *J. Elect. Eng. Technol*., Vol. 10, No. 5, pp. 1989-2000, Sep. 2015.

[7] N. Femia, G. Lisi, G. Petrone, G. Spagnuolo, and M. Vitelli, "Distributed maximum power point tracking of photovoltaic arrays: Novel approach and system analysis," *IEEE Trans. Ind. Electron*., Vol. 55, No. 7, pp. 2610-2621, Jul. 2008.

[8] C. Olalla, D. Clement, M. Rodriguez, and D. Maksimovic, "Architectures and control of submodule integrated dc-dc converters for photovoltaic applications," *IEEE Trans. Power Electron*., Vol. 28, No. 6, pp. 2980-2997, Jun. 2013.

[9] S. Qin, S. T. Cady, A. D. Dominguez-Garcia, and R. C. N. Pilawa-Podgurski, "A distributed approach to maximum power point tracking for photovoltaic submodule differential power processing," *IEEE Trans. Power Electron*., Vol. 30, No. 4, pp. 2024-2040, Apr. 2015.

[10] R. Bell and R. C. N. Pilawa-Podgurski, "Decoupled and distributed maxi-mum power point tracking of series-connected photovoltaic sub-modules using differential power processing," *IEEE J. Emerg. Sel. Topics Power Electron*., Vol. 3, No. 4, pp. 881-891, Dec. 2015.

[11] T. Thang, N. Thao, J.-H. Jang, and J.-H. Park, "Analysis and design of grid-connected photovoltaic systems with multiple-integrated converters and a pseudo-dc-link inverter," *IEEE Trans. Ind. Electron*., Vol. 61, No. 7, pp. 3377-3386, Jul. 2014.

[12] J. H. Park, J.-Y. Ahn, B.-H. Cho, and G.-J. Yu, "Dual-module-based maximum power point tracking control of photovoltaic systems," *IEEE Trans. Ind. Electron*., Vol. 53, No. 4, pp. 1036-1047, Jun. 2006.

[13] A. Ahmed, P. Ganeshkumar, J.-H. Park, and H. Lee, "FPGA-based centralized controller for multiple PV generators tied to the dc bus," *J. Power Electron*., Vol. 14, No. 4, pp. 733-741, Jul. 2015.

[14] K. A. Kim, P. S. Shenoy, and P. T. Krein, "Converter rating analysis for photovoltaic differential power processing systems," *IEEE Trans. Power Electron*., Vol. 30, No. 4, pp. 1987-1997, Apr. 2015.

[15] Y.-T. Jeon and J.-H. Park, "Frequency-PWM hybrid controller of single-switch forward-flyback converter for DC-link regulation of 27-level cascaded H-bridge inverter," *IEICE Electronics Express*, Vol. 14, No. 13, 2017.

[16] J.-H. Park, H.-W. Kim, and J.-H. Park, "Magnetically-coupled boost-forward converter for high efficiency differential power processing systems," *IEICE Electronics Express* Vol. 14, No. 3, 2017.

[17] J.-H. Park, K. T. Kim, and J.-H. Park, "Continuous conduction mode coupled-inductor buck-flyback converter for charge balancing," *KIEE Spring Conference*, pp. 228-230, 2015.

Chun-Gu Lee received his B.S. degree from the Department of Electrical Engineering of Soongsil University, Seoul, Korea, in 2015, where he is presently working towards his combined Master-Ph.D. degree. His current research interests include the analysis and design of differential power processing converters and renewable energy applications.

Jung-Hyun Park received his B.S. and M.S. degrees from the Department of Electrical Engineering of Soongsil University, Seoul, Korea, in 2015 and 2017, respectively. His current research interests include the analysis and design of differential power processing converters and renewable energy applications.

Joung-Hu Park received his B.S., M.S. and Ph.D. degrees from the Department of Electrical Engineering and Computer Science of Seoul National University, Seoul, Korea, in 1999, 2001 and 2006, respectively. He was a Visiting Scholar at the Center for Power Electronics Systems, Virginia Polytechnic Institute and State University, Blacksburg, VA, USA, from 2004 to 2005. He was a Visiting Professor at the University of British Columbia, Vancouver, BC, Canada, from 2015 to 2016. He is presently working as an Associate Professor at Soongsil University, Seoul, Korea.